Supporting Information

Leveraging Temperature-Tunable, Scale-like Microstructure to Produce Multimodal, Supersensitive Sensors

Yanlong Tai[1,2], Tushar Kanti Bera[1], Zhenguo Yang[2*], Gilles Lubineau[1*]

[1] King Abdullah University of Science and Technology (KAUST), Division of Physical Science and Engineering, COHMAS Laboratory, Thuwal 23955-6900, Saudi Arabia
[2] Fudan University, Department of Materials Science, Shanghai 200433, China.

* Corresponding authors
Email: zgyang@fudan.edu.cn (Zhenguo Yang), gilles.lubineau@kaust.edu.sa (Gilles, lubineau)

This PDF file includes:

1. Experimental videos.

Video-S1: Continuous monitoring of a human wrist and signals via a SSPF-based sensing device.
Video-S2: The homogeneous and rapid response to temperature by a SSPF-2.
Video-S3: Application of SSPF-2 for monitoring temperature and as a thermal switch (a fire alarming system).
Video-S4: Application of SSPF-2 for monitoring light and as a light switch via a temperature mechanism.

2. Figure S1, Figure S2, and Figure S3: Further characterization of WSPFs and SSPFs.

3. Table S1, Table S2, Figure S4, and Figure S5: A summary of the recent literature about flexible pressure-sensing systems and temperature-sensing materials.
4. Figure S6: Response of SSPFs to light via a temperature mechanism.
5. Figure S7 and Figure S8: Analysis of the sensing mechanism of SSPFs.
6. Figure S9, Figure S10, Figure S11, Figure S12: Experimental Method.
7. References

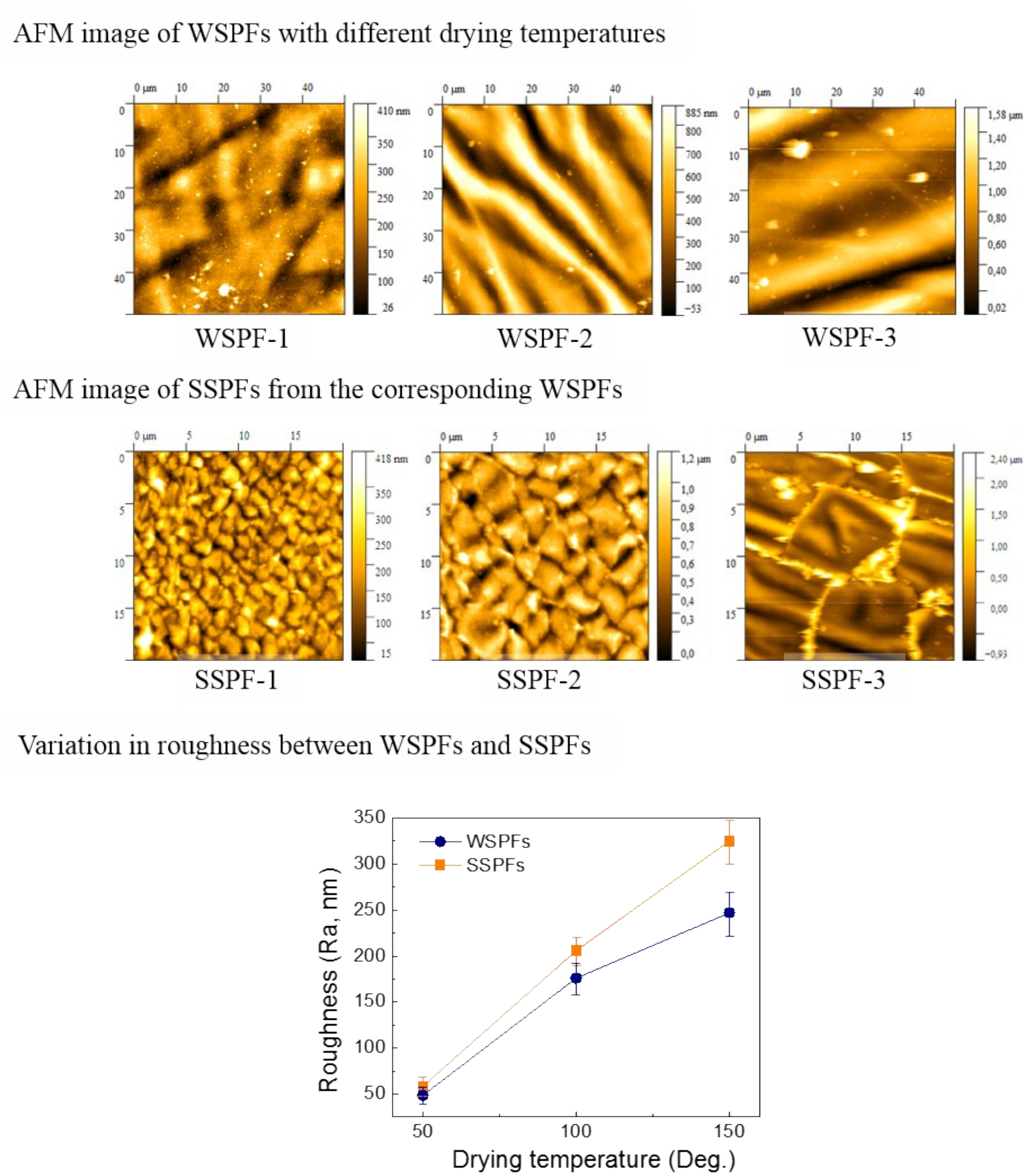

Figure S1. Atomic Force Microscope (AFM) images comparing the roughness between WSPFs and SSPFs.

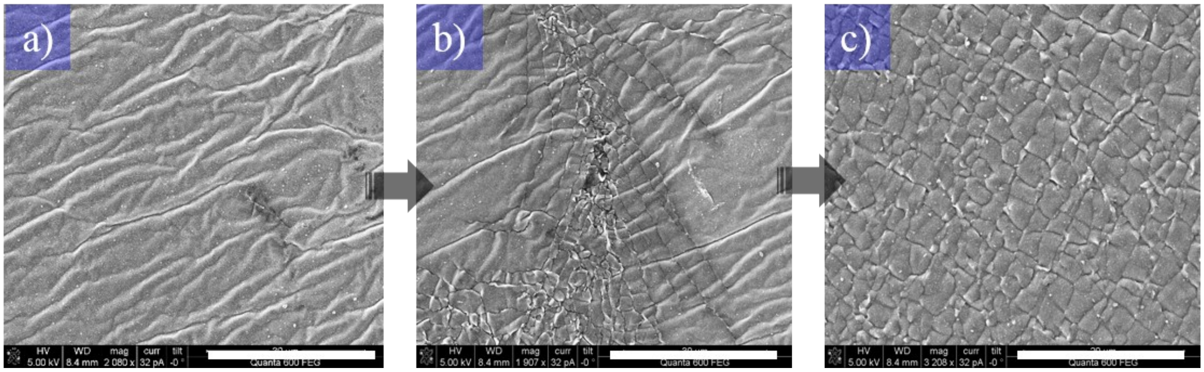

Figure S2. The typical crack formation process from WSPF-2 to SSPF-2. a) WSPF-2; b) beginning of the cracking process; c) SSPF-2. All scale bars are 20 μm.

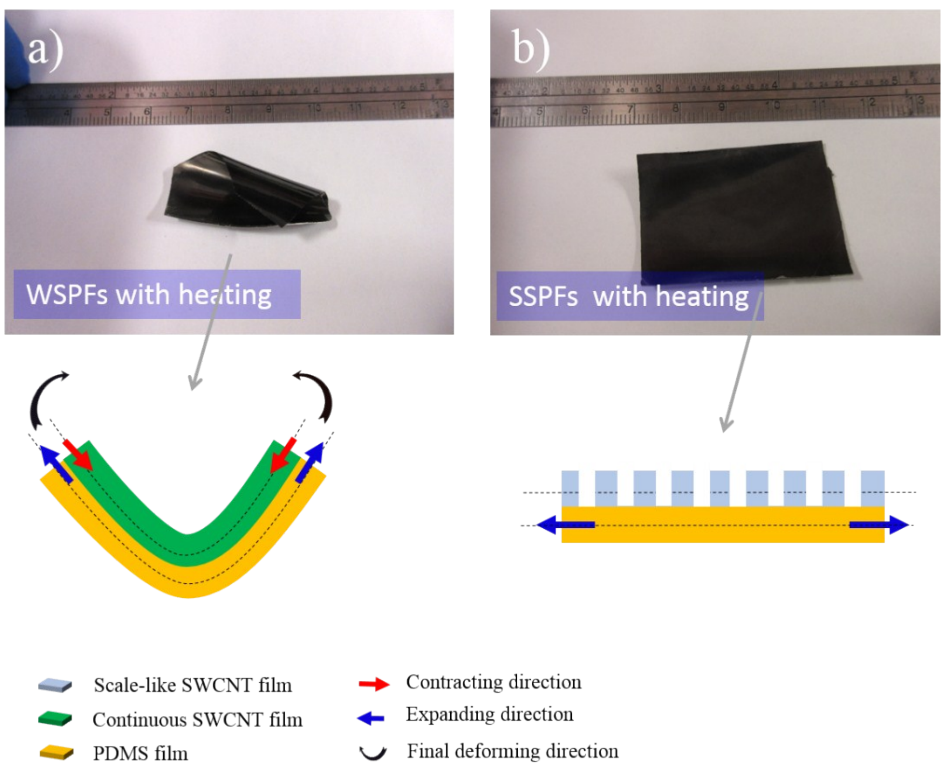

Figure S3. The thermal deformation of a) WSPF-2, which bends due to its CTE value (PDMS: expansion, SWCNT: contraction) and b) SSPF-2, which has a fragmentation to its coating, as well as the corresponding illustration of deformations. The temperature was set at 100 °C.

Table S1. A summary of the key responses of SSPFs to variation in pressure.

Sample [a]	R_0 (10^3, ohm)	Pressure/90% (break, kPa)[b]	ΔR/90% (10^6, ohm)	Sensitivity (break, kPa^{-1}) [c]	Effective sensitivity (kPa^{-1})[d]
SSPF-1	13.2	45/40.5	27.7/19.5	46.6	36.5
SSPF-2	2	63/56.7	35.1/24.6	278.6	216.9
SSPF-3	0.6	81/72.9	44.9/32.4	923.9	740.7

[a]: Sample size = a circle film with a diameter of 8 mm, and silver as electrode;

[b]: We define that the preferred detecting scope is 90 % of its breaking pressure load;

[c]: The sensitivity is defined as $\Delta R/R_0$ to pressure;

[d]: The effective sensitivity is calculated from 90 % of its breaking pressure load with the corresponding variation in resistance.

Note that all data are the average values taken from three samples.

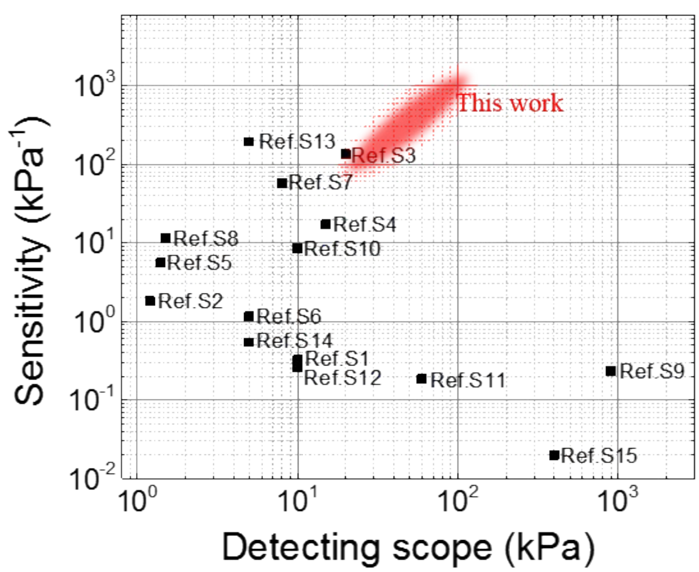

Figure S4. A summary of the recent literature with the key parameters for flexible pressure-sensing systems.

Table S2. A summary of the key parameters of SSPFs to variation in temperature.

Sample	R_0 (10^3, ohm)[a]	Tem./90% (break, ℃)[b]	R/90% (break, 10^6, ohm)	Thermal Index (break, 10^3, K)[c]	Effective Thermal Index (10^3, K^{-1})[d]
SSPF-1	13.2	56.2/50.6	27.7/19.5	29.9	29.9
SSPF-2	2	73.2/65.9	35.1/24.6	20.4	20.4
SSPF-3	0.6	86.7/78	44.9/32.4	17.6	17.6

[a]: Sample size = a circle film with a diameter of 8 mm and with silver as the electrode;

[b]: We define that the preferred detecting scope is 90 % of its breaking temperature;

[c]: The sensitivity is calculated according to Eq. 3;

[d]: The effective sensitivity is calculated from 90 % of its breaking temperature with the corresponding variation in resistance.

Note that all data are the average values taken from three samples.

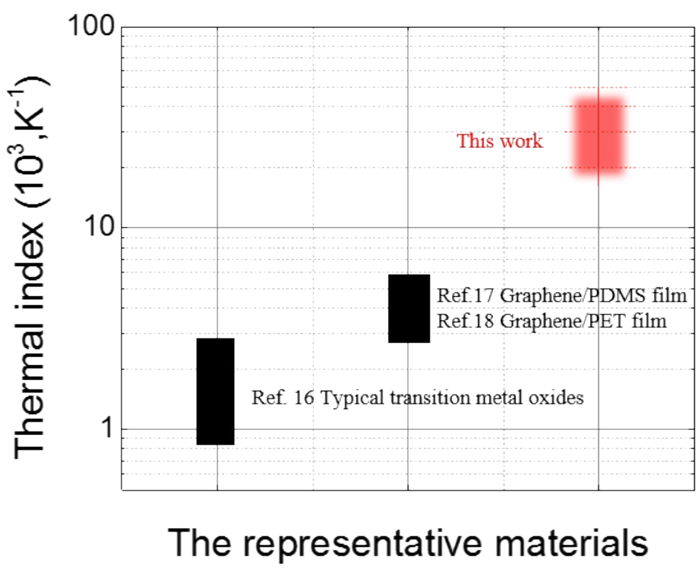

Figure S5. A summary of the recent literature with the key parameters for temperature-sensing materials.

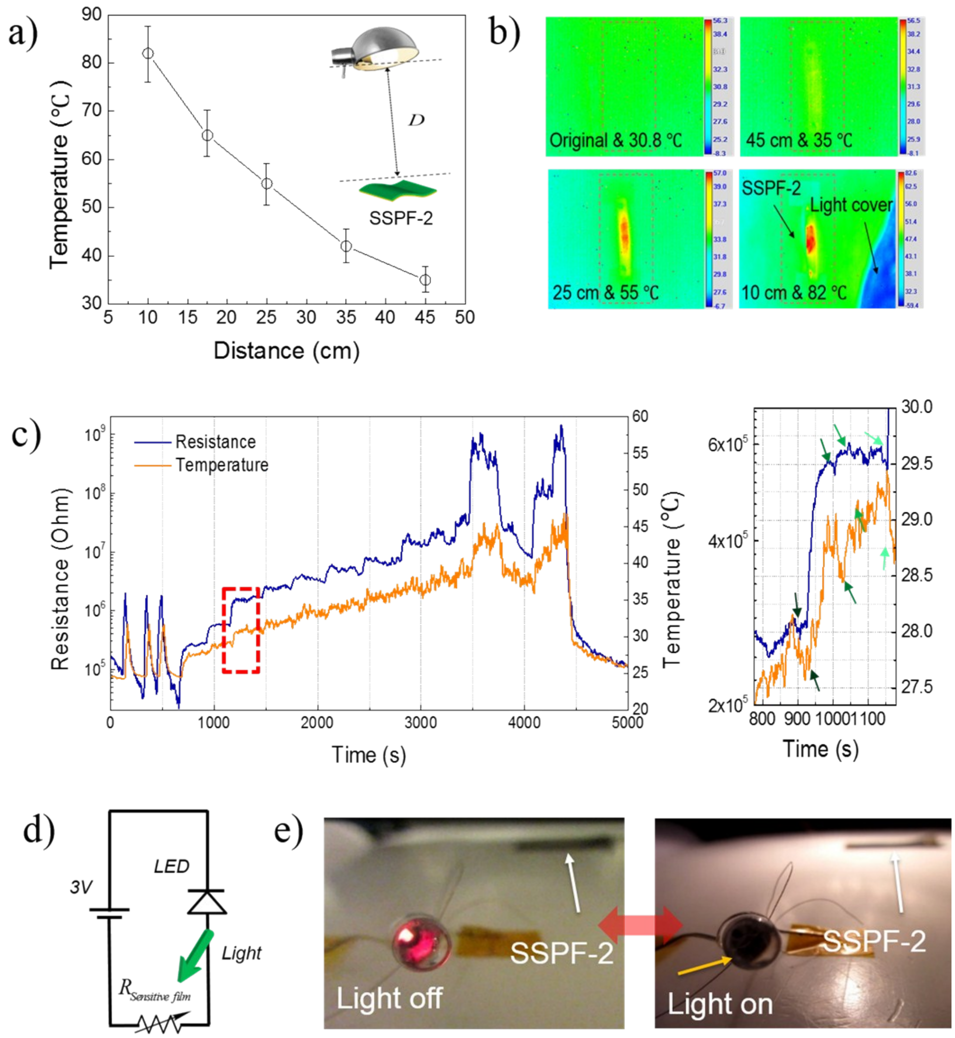

Figure S6. The response of SSPF-2 to light. a) Relationship between temperature of SSPF-2 and distance from a light; b) the temperature distribution of the film with different distances from the light; c) light-monitoring performance; d) equivalent circuit and digital images for demonstrating the efficiency of SSPF-2 as a light switch. Note that the light is 100 W and the default distance is 10 cm.

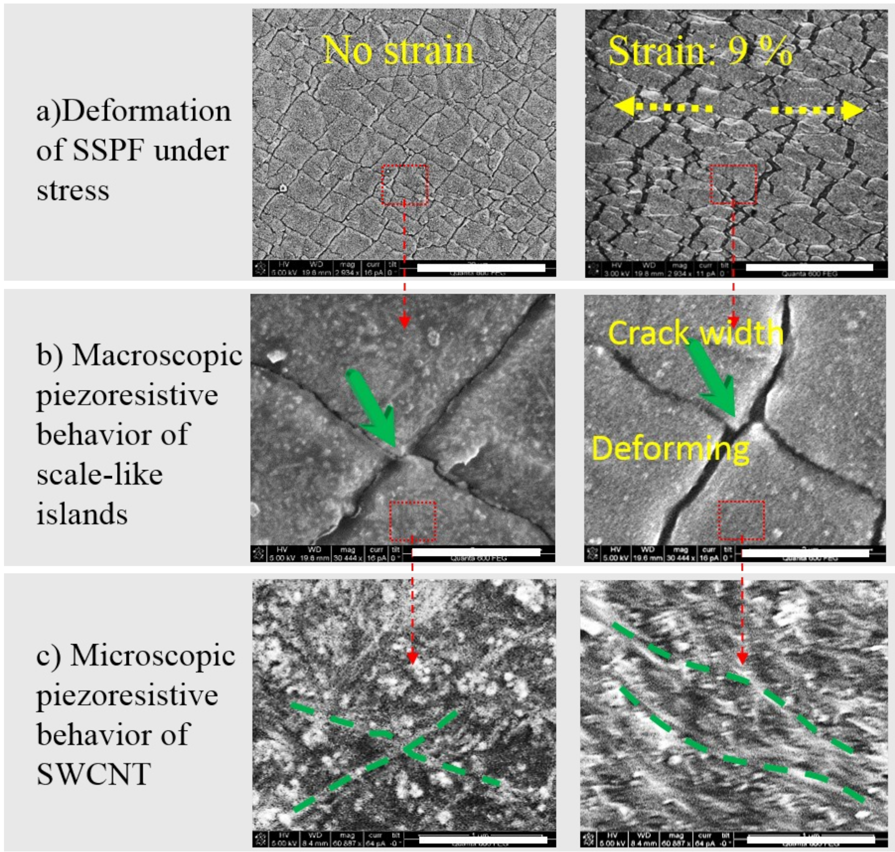

Figure S7. SEM images illustrating the sensing mechanism of SSPFs. a) Deformation of SSPF without strain and with strain; the scale bar is 20 µm. b) Macroscopic piezoresistive behavior of SSIs; the scale bar is 1 µm. c) Microscopic piezoresistive behavior of SWCNT bundles; the scale bar is 500 nm.

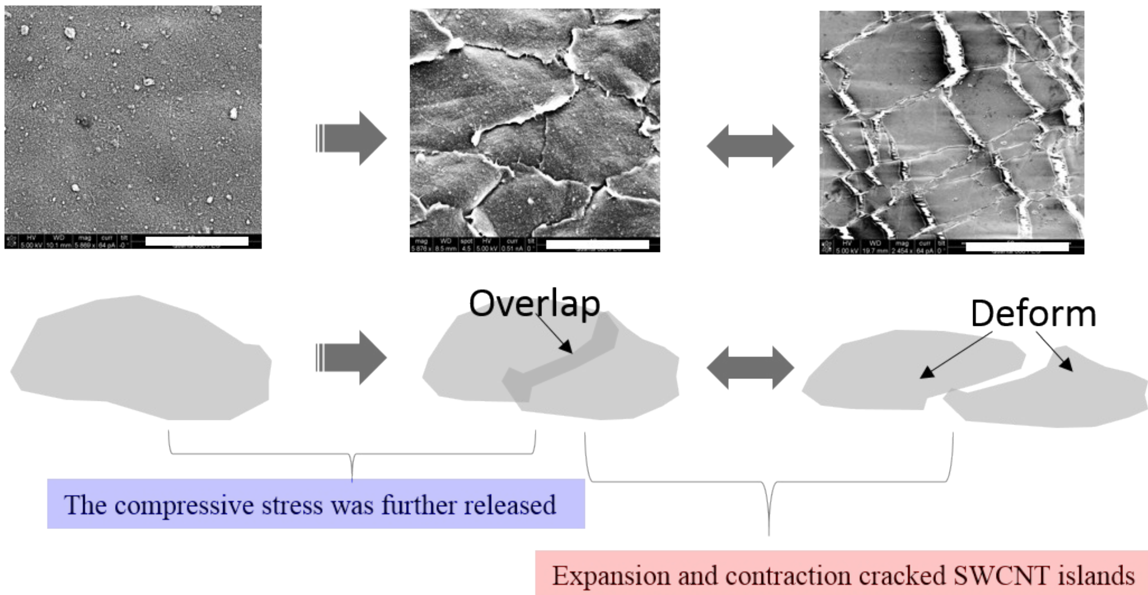

Figure S8. SEM images and illustration for the evolution to WSPF transforming to SSPF and the deformation of SSPFs. All scale bars are 20 μm.

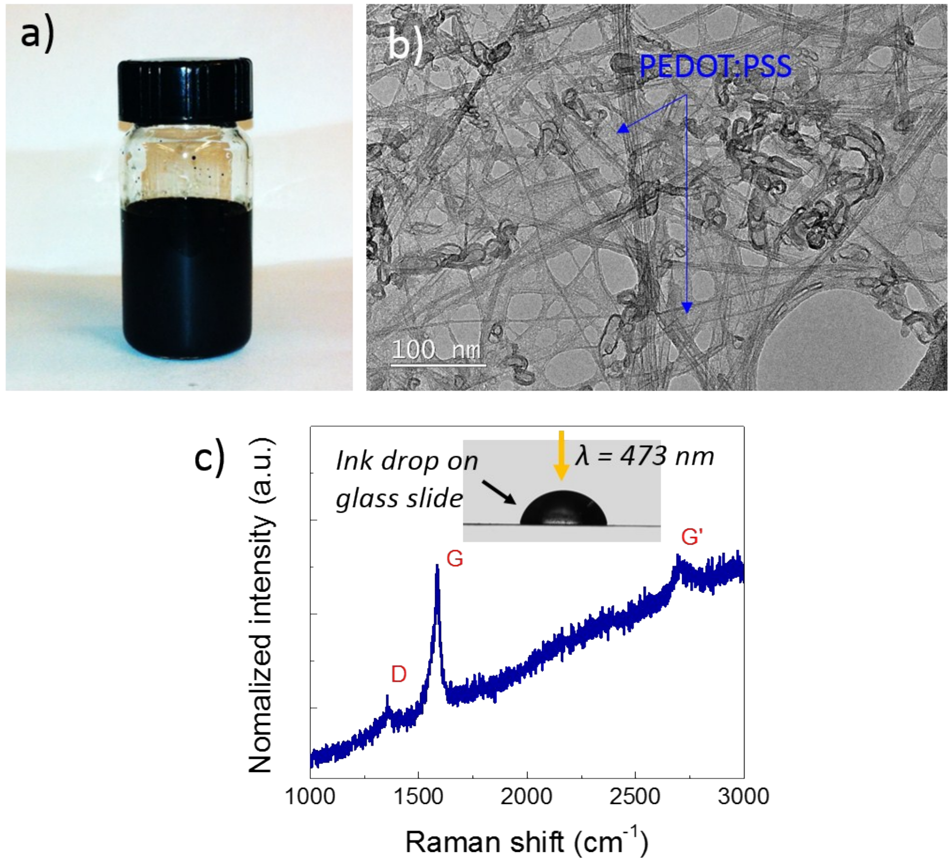

Figure S9. a) Typical SWCNT ink (1 mg/ml); b) TEM of SWCNTs; c) Raman spectra with D, G, and G’ band peaks, indicating the high purity of SWCNT. Note that the curve is generated directly from the ink sample, as shown by the inset image.

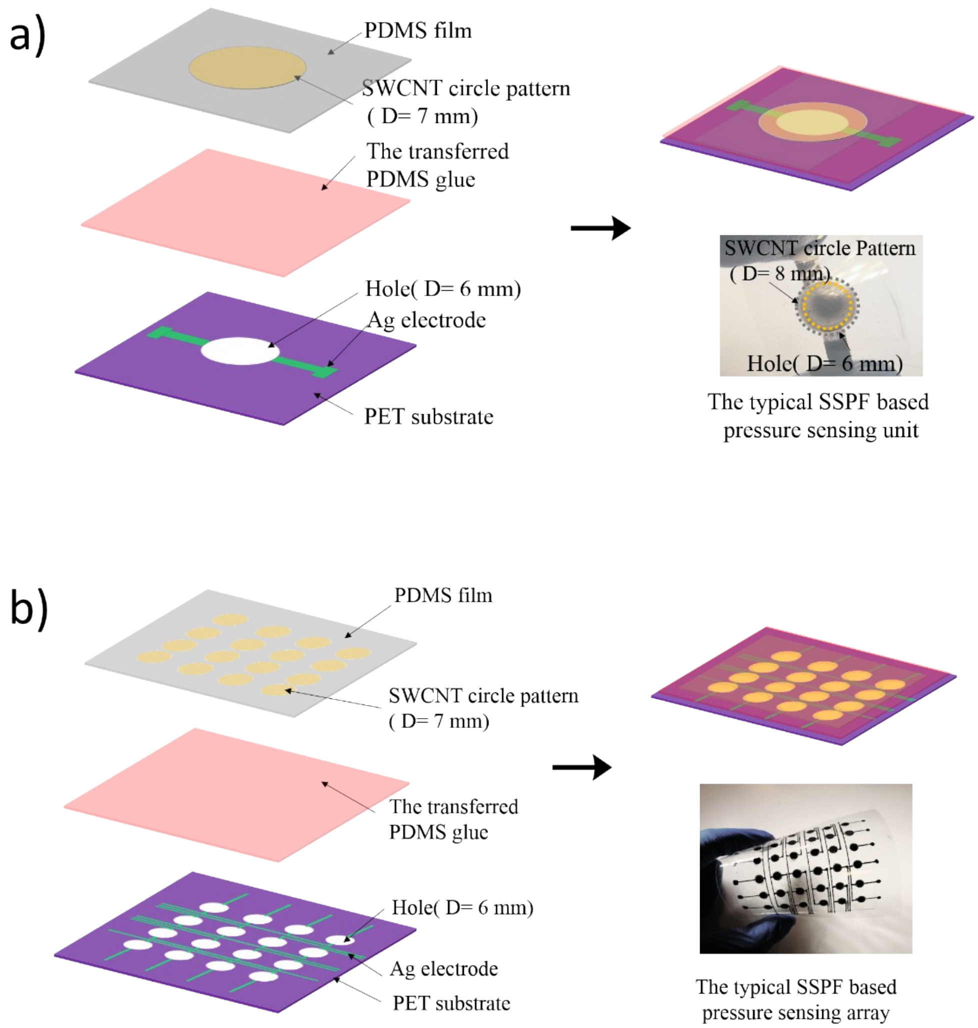

Figure S10. Scheme illustrations of the fabrication of SSPF-based pressure-sensing systems and the digital images of the typical devices a) as a unit and b) as an array.

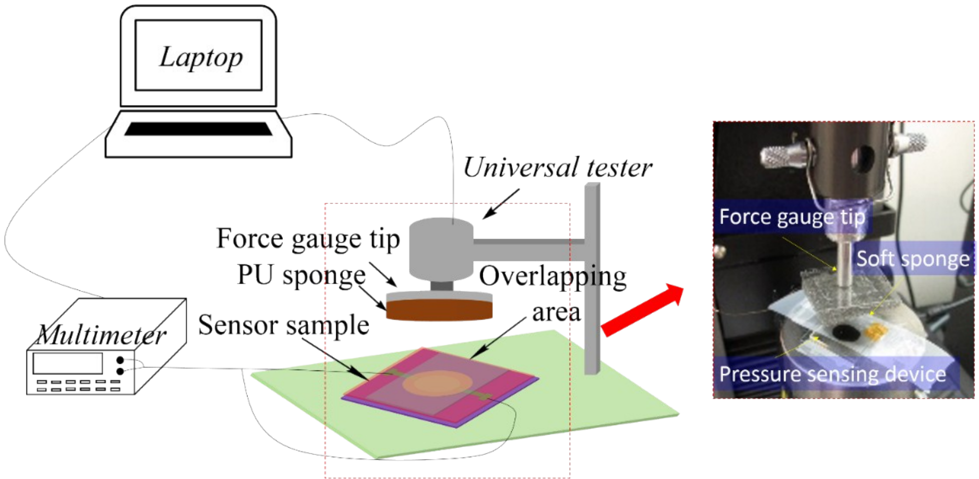

Figure S11. Illustration and digital image of the setups used to test the sensitivity of films to mechanical pressure.

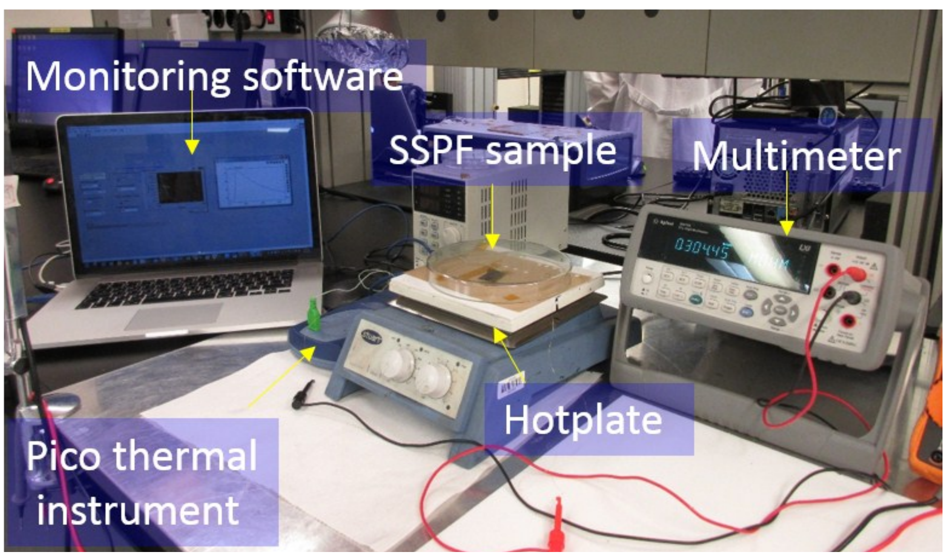

Figure S12. Digital image of the setups used to test for sensitivity to temperature.

Supporting Reference

1. Yao, H.B., Ge, J., Wang, C.F., Wang, X., Hu, W., Zheng, Z.J., Ni, Y. and Yu, S.H., 2013. A flexible and highly pressure-sensitive graphene–polyurethane sponge based on fractured microstructure design.*Advanced Materials*, *25*(46), pp.6692-6698.
2. Wang, X., Gu, Y., Xiong, Z., Cui, Z. and Zhang, T., 2014. Silk-molded flexible, ultrasensitive, and highly stable electronic skin for monitoring human physiological signals. *Advanced Materials*, *26*(9), pp.1336-1342.
3. Pan, L., Chortos, A., Yu, G., Wang, Y., Isaacson, S., Allen, R., Shi, Y., Dauskardt, R. and Bao, Z., 2014. An ultra-sensitive resistive pressure sensor based on hollow-sphere microstructure induced elasticity in conducting polymer film. *Nature communications*, *5*.
4. Shao, Q., Niu, Z., Hirtz, M., Jiang, L., Liu, Y., Wang, Z. and Chen, X., 2014. High-Performance and Tailorable Pressure Sensor Based on Ultrathin Conductive Polymer Film. *Small*, *10*(8), pp.1466-1472.
5. Zhu, B., Niu, Z., Wang, H., Leow, W.R., Wang, H., Li, Y., Zheng, L., Wei, J., Huo, F. and Chen, X., 2014. Microstructured graphene arrays for highly sensitive flexible tactile sensors. *Small*, *10*(18), pp.3625-3631.
6. Gong, S., Schwalb, W., Wang, Y., Chen, Y., Tang, Y., Si, J., Shirinzadeh, B. and Cheng, W., 2014. A wearable and highly sensitive pressure sensor with ultrathin gold nanowires. *Nature communications*, *5*.
7. Choong, C.L., Shim, M.B., Lee, B.S., Jeon, S., Ko, D.S., Kang, T.H., Bae, J., Lee, S.H., Byun, K.E., Im, J. and Jeong, Y.J., 2014. Highly stretchable resistive pressure sensors using a conductive elastomeric composite on a micropyramid array. *Advanced Materials*, *26*(21), pp.3451-3458.
8. Pang, C., Lee, G.Y., Kim, T.I., Kim, S.M., Kim, H.N., Ahn, S.H. and Suh, K.Y., 2012. A flexible and highly sensitive strain-gauge sensor using reversible interlocking of nanofibres. *Nature materials*, *11*(9), pp.795-801.
9. Lipomi, D.J., Vosgueritchian, M., Tee, B.C., Hellstrom, S.L., Lee, J.A., Fox, C.H. and Bao, Z., 2011. Skin-like pressure and strain sensors based on transparent elastic films of carbon nanotubes. *Nature nanotechnology*,*6*(12), pp.788-792.
10. Schwartz, G., Tee, B.C.K., Mei, J., Appleton, A.L., Kim, D.H., Wang, H. and Bao, Z., 2013. Flexible polymer transistors with high pressure sensitivity for application in electronic skin and health monitoring. *Nature communications*, *4*, p.1859.
11. Chen, Z., Ming, T., Goulamaly, M.M., Yao, H., Nezich, D., Hempel, M., Hofmann, M. and Kong, J., 2016. Enhancing the Sensitivity of Percolative Graphene Films for Flexible and Transparent Pressure Sensor Arrays.*Advanced Functional Materials*.

12. Luo, N., Dai, W., Li, C., Zhou, Z., Lu, L., Poon, C.C., Chen, S.C., Zhang, Y. and Zhao, N., 2016. Flexible Piezoresistive Sensor Patch Enabling Ultralow Power Cuffless Blood Pressure Measurement. *Advanced Functional Materials*, *26*(8), pp.1178-1187.
13. Zang, Y., Zhang, F., Huang, D., Gao, X., Di, C.A. and Zhu, D., 2015. Flexible suspended gate organic thin-film transistors for ultra-sensitive pressure detection. *Nature communications*, *6*.
14. Pang, C., Koo, J.H., Nguyen, A., Caves, J.M., Kim, M.G., Chortos, A., Kim, K., Wang, P.J., Tok, J.B.H. and Bao, Z., 2015. Highly Skin-Conformal Microhairy Sensor for Pulse Signal Amplification. *Advanced Materials*,*27*(4), pp.634-640.
15. Yeo, J.C., Yu, J., Loh, K.P., Wang, Z. and Lim, C.T., 2016. Triple-state liquid-based microfluidic tactile sensor with high flexibility, durability, and sensitivity. *ACS Sensors*, *1*(5), pp.543-551.
16. Feteira, A. Negative Temperature Coefficient Resistance (NTCR) Ceramic Thermistors: An Industrial Perspective. J. Am. Ceram. Soc. 2009, 92, 967.
17. Shahil, K. M. F.; Balandin, A. A. Thermal Properties of Graphene and Multilayer Graphene: Applications in Thermal Interface Materials. Solid State Commun. 2012, 152, 1331.
18. Yan, C., Wang, J. and Lee, P.S., 2015. Stretchable graphene thermistor with tunable thermal index. ACS nano, 9(2), pp.2130-2137.